Aaron et al. Geoenvironmental Disasters (2017) 4:5
DOI 10.1186/s40677-017-0070-4

Geoenvironmental Disasters

RESEARCH Open Access

The role of initial coherence and path materials in the dynamics of three rock avalanche case histories

Jordan Aaron[1*], Scott McDougall[1], Jeffrey R. Moore[2], Jeffrey A. Coe[3] and Oldrich Hungr[1]

Abstract

Background: Rock avalanches are flow-like landslides that can travel at extremely rapid velocities and impact surprisingly large areas. The mechanisms that lead to the unexpected mobility of these flows are unknown and debated. Mechanisms proposed in the literature can be broadly classified into those that rely on intrinsic characteristics of the rock avalanche material, and those that rely on extrinsic factors such as path material. In this work a calibration-based numerical model is used to back-analyze three rock avalanche case histories. The results of these back-analyses are then used to infer factors that govern rock avalanche motion

Results: Our study has revealed two key insights that must be considered when analyzing rock avalanches. Results from two of the case histories demonstrate the importance of accounting for the initially coherent phase of rock avalanche motion. Additionally, the back-analyzed basal resistance parameters, as well as the best-fit rheology, are different for each case history. This suggests that the governing mechanisms controlling rock avalanche motion are unlikely to be intrinsic. The back-analyzed strength parameters correspond well to those that would be expected by considering the path material that the rock avalanches overran.

Conclusion: Our results show that accurate simulation of rock avalanche motion must account for the initially coherent phase of movement, and that the mechanisms governing rock avalanche motion are unlikely to be intrinsic to the failed material. Interaction of rock avalanche debris with path materials is the likely mechanism that governs the motion of many rock avalanches.

Background

Rock avalanches are a class of extremely rapid, flow-like landslides that can impact people and property far from their source. Beginning with the work of Heim (1932), many researchers have noted an apparent increase in rock avalanche mobility with increasing volume (Heim 1932; Scheidegger 1973; Hsu 1975; Li 1983; Corominas 1996; Legros 2006; Whittall et al. 2016). This observation is based on plots of volume vs. angle of reach (defined as the inclination from horizontal of the line connecting the highest point on the failure scarp to the distal end of the deposit), suggesting that higher volume events have greater mobility. However, the mechanism(s) that contribute(s) to this apparent volume-mobility trend remain debated (e.g. Hungr and Evans, 2004).

A number of theories have been proposed to explain the apparent correlation between mobility and volume of rock avalanches. Many of these theories are reviewed by Legros (2002) and Hungr & Evans (2004). The theories can be broadly grouped into mechanisms that are due to intrinsic characteristics of the rock avalanche material and those that rely on extrinsic factors such as path material. The following recently published theories demonstrate that the debate surrounding rock avalanche movement mechanisms is still ongoing. These include:

- Johnson et al. (2016) showed results of discrete particle models that predict an increase of mobility with increasing volume. They propose that this phenomenon arises from acoustic waves propagating through the particle assembly that reduce

* Correspondence: jaaron@eos.ubc.ca
[1]Department of Earth, Ocean and Atmospheric Sciences, University of British Columbia, 2020 - 2207 MainMall, Vancouver, British Columbia V6T 1Z4, Canada
Full list of author information is available at the end of the article

intergranular stresses, consistent with the theory of acoustic fluidization (e.g. Melosh 1979).
- Manzanal et al. (2016) proposed that rock avalanches dilate upon failure, however; as fragmentation proceeds, the reduction in grain size results in a switch from dilative to contractive behaviour, resulting in generation of pore-air pressures.
- Lucas et al. (2014) proposed a velocity weakening rheology, and showed that a consistent set of parameters could reproduce field observations from three rock avalanche case histories. They noted that their rheology is consistent with the mechanism of flash heating.
- Bowman et al. (2012) presented geotechnical centrifuge experiments that suggest a positive correlation between degree of fragmentation and runout length. Their experiments used a bilinear path with a high angle sloped portion (70°). Blasio & Crosta (2015) demonstrated that a steep path combined with isotropic fragmentation can increase centre of mass displacement; however, the effect disappears for slope angles typical of rock avalanche paths.
- Coe et al. (2016) and Aaron & Hungr (2016a) both invoked low basal friction due to entrainment and overriding of saturated soil to explain the dynamics of the West Salt Creek rock avalanche and the Avalanche Lake rock avalanche, respectively. In both cases, this hypothesis was supported by field evidence of entrained path material at the base of the deposit.

Due to the uncertainty about the governing mechanisms contributing to rock avalanche motion, the development of mechanistic models remains challenging. Instead, many researchers use semi-empirical models (e.g. Hungr 1995). In these models, the governing equations are derived based on conservation of mass and momentum; however, the parameters that govern the simulations are not true material properties. Instead, these parameters are empirical and derived based on back-analysis of full-scale case histories. These models typically treat the rock avalanche as a frictional fluid, which ignores the effects of the initially coherent stage of rock avalanche motion (Aaron & Hungr 2016b).

Over the past two decades, there has been a proliferation of models developed based on a semi-empirical approach (Bouchut et al. 2003; Pitman et al. 2003; McDougall & Hungr 2004; Pirulli 2005; Pastor et al. 2009; Huang et al. 2012; Cascini et al. 2014; Dai et al. 2014). These models work well in a back-analysis context; however, they have only been applied to forecast potential runout in a few published cases (e.g. Nicol et al. 2013; Loew et al. 2017). The challenge of performing forward-analysis with these models is that it remains difficult to relate successful back-analyses to potential failures. This is the biggest challenge that must be overcome before semi-empirical runout models can be routinely used in practice, and arises from the fact that there are likely multiple mechanisms that govern mobility and the conditions contributing to these mechanisms are usually not known a priori.

The purpose of this study is to investigate factors governing rock avalanche motion using two dynamic models. We show that many characteristics of rock avalanche motion can be explained by considering the disintegration process and the slide path materials. We first provide a description of the dynamic models used for this investigation in the following section, then describe results of our back-analyses of three large-volume rock avalanches.

Description of the dynamic models

Two dynamic models, entitled the flexible block model (Aaron and Hungr, 2016b) and Dan3D (McDougall, 2006; Hungr and McDougall, 2009) are used in the present work. These models each describe different phases of rock avalanche motion. The flexible block model is appropriate for simulating the initially coherent portion of rock avalanche motion, while Dan3D is used to simulate the rock avalanche motion after it fragments and becomes flow-like. The key aspects of these two models are described in the following sections.

Flexible block model

The flexible block model is a dynamic model developed to simulate the initially coherent phase of motion exhibited by many rock avalanches. In this model, the landslide is treated as a flexible block that translates and rotates over a user-defined, three-dimensional rupture surface. Movement is initiated by an unbalanced gravitational force accelerating the failed material from rest. Deformation is not permitted in the horizontal directions; however, vertical deformation is allowed in order to ensure that the flexible block remains on the rupture surface. The governing equations solved by this model are shown in Eqs. 1, 2 and 3. A detailed derivation of these equations is presented by Aaron & Hungr (2016b). The flexible block model uses an orthogonal coordinate system with the z-axis oriented vertically.

$$m_{body} * \dot{v}_x = F_x \tag{1}$$

$$m_{body} * \dot{v}_y = F_y \tag{2}$$

$$I_z * \dot{\omega}_z = T_z \tag{3}$$

Where m_{body} is the mass of the flexible block, $\dot{v}_x$, $\dot{v}_y$ are the x and y translational accelerations, F_x, F_y are the net forces acting on the flexible block in the x and y directions, I_z is the moment of inertia of the flexible block taken about the z-axis, $\dot{\omega}_z$ is the angular acceleration

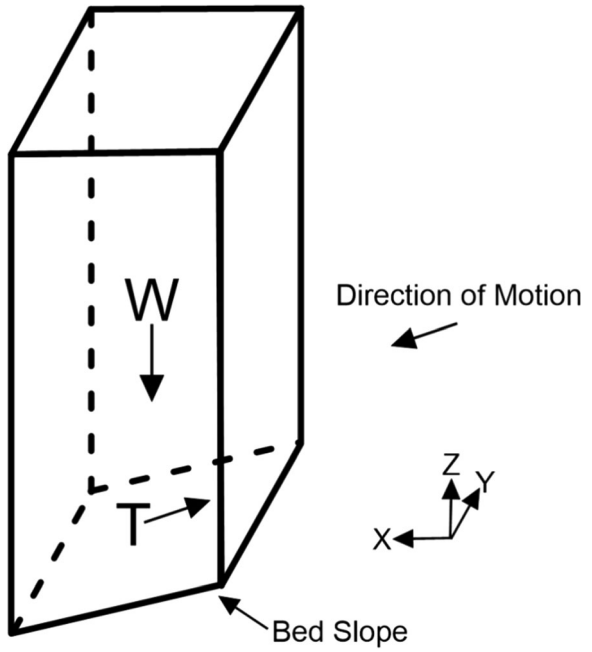

Fig. 1 Forces acting on a column of material in the flexible block model. W is the weight of the column, and T is the basal resistance force

about the vertical z-axis, and T_z is the net torque acting about the z-axis.

The net force and torque on the flexible block are calculated by discretizing the failed mass into a system of columns. The number of columns used to represent the failed mass can either be chosen by the user or selected automatically based on the resolution of the input topography files. As shown in Fig. 1, the forces resolved on each column are the column weight and the basal resistance force which acts opposite the direction of motion. The net forces acting on each column are summed to derive the net force and torque acting on the assemblage of columns. This algorithm is summarized in Fig. 2. This procedure is similar to simple 3D limit-equilibrium methods (methods which neglect internal forces); however, instead of solving for a factor of safety, the method solves for translational and angular accelerations. In the current version of the model, internal forces are neglected, so the model should not be used to simulate strongly compound failures.

Dan3D

The governing equations solved by Dan3D are summarized in Eqs. 4 and 5 (McDougall 2006). Only the final form of the equations used in the model are presented; a detailed derivation is presented by Hungr & McDougall (2009). These equations are depth-averaged and derived in

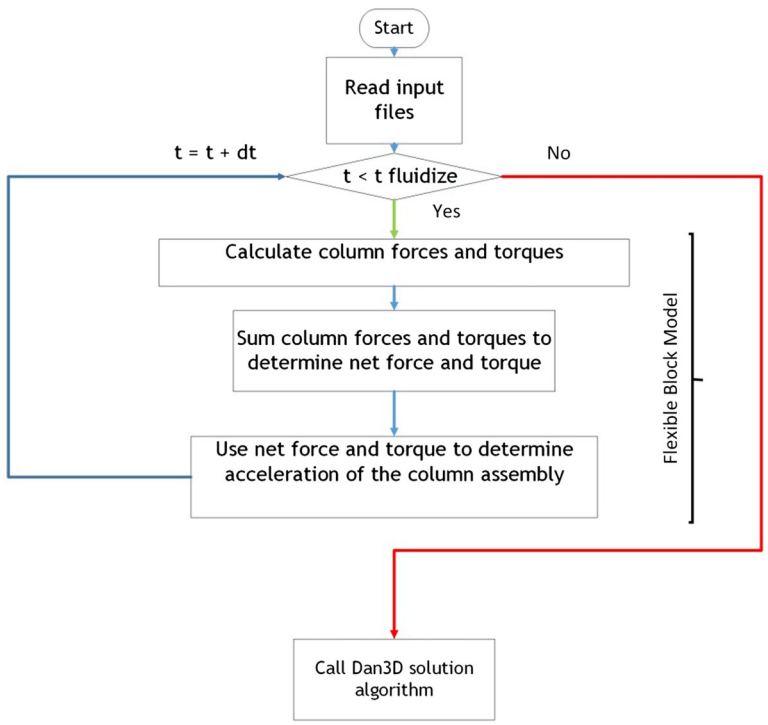

Fig. 2 Flowchart of the flexible block model algorithm. The three steps that describe the flexible block model are highlighted. t fluidize is a user specified parameter

a Lagrangian coordinate system, with the x-coordinate aligned with the local direction of motion and the z-coordinate oriented in the bed-normal direction.

$$\rho h \frac{Dv_x}{Dt} = \rho h g_x - k_x \sigma_z \frac{\partial h}{\partial x} + \tau_{zx} - \rho v_x E \tag{4}$$

$$\rho h \frac{Dv_y}{Dt} = \rho h g_y - k_y \sigma_z \frac{\partial h}{\partial y} \tag{5}$$

Where ρ is the density, $v_{x,y}$ are the depth-averaged x and y velocities, h is the flow depth, $g_{x,y}$ are the x and y components of gravity, $k_{x,y}$ are the x and y horizontal stress ratios (ratio of lateral stress to bed normal stress) calculated based on Savage-Hutter theory (Savage and Hutter, 1989), σ_z is the bed normal stress, τ_{zx} is the basal resistance, and E is the entrainment rate.

A free-body diagram that shows the forces acting on a slice of material oriented in the direction of motion is displayed in Fig. 3. The first term on the right hand side of Eqs. 4 and 5 represents the gravitational stress (the downslope component of the W force in Fig. 3), while the second term represents the longitudinal pressure gradient (P force in Fig. 3). The basal resistance stress (T force in Fig. 3) and momentum loss due to entrainment (E force in Fig. 3) only occur in the x-direction due to the fact that the x-coordinate is aligned with the local direction of motion. The entrainment rate (E) and density, as well as the parameters that govern $k_{x,y}$ and τ_{zx}, are user-specified.

When performing a back analysis with Dan3D, the parameters that are commonly calibrated are the internal friction angle (used to calculate $k_{x,y}$) and parameters associated with the user-specified basal rheology (used to calculate τ_{zx}). The entrainment rate is sometimes a calibrated parameter, although it is common to evaluate this parameter based on known estimates of initial and final volumes (McDougall & Hungr, 2005).

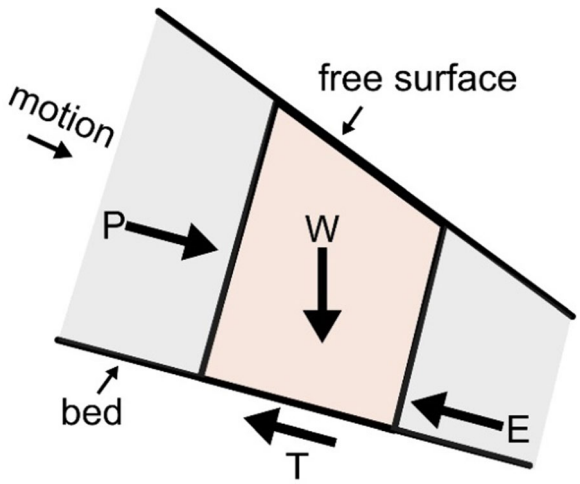

Fig. 3 Conceptual free-body diagram of a slice of material oriented in the direction of motion in Dan3D. W is the weight; T is the basal resistance; P is the internal force due to free surface gradients; and E is the inertial resistance due to entrainment

Three rheologies are commonly used in Dan3D simulations to calculate τ_{zx}. The frictional rheology is shown in Eq. 6:

$$\tau_{zx} = -\sigma_z \tan(\varnothing_b) \tag{6}$$

where σ_z is the bed-normal effective stress and $\varnothing_b$ is the calibrated apparent friction angle, which includes pore-pressure effects. The Voellmy rheology (e.g. Hungr & McDougall, 2009), given in Eq. 7 is similar to the frictional rheology, with an additional velocity-dependent term:

$$\tau_{zx} = \left(-\sigma_z f + \frac{\rho g v_x^2}{\xi}\right) \tag{7}$$

where f is the friction coefficient (equivalent to tan ($\varnothing_b$)) and ξ is the turbulence parameter. Both f and ξ are calibrated parameters. The Bingham rheology (e.g. Hungr & McDougall, 2009), given by Eq. 8, does not assume that the basal resistance is proportional to the bed-normal effective stress:

$$\tau_{zx}^3 + 3\left(\frac{\tau_{yield}}{2} + \frac{\mu_{Bingham} v_x}{h}\right)\tau_{zx}^2 - \frac{\tau_{yield}^3}{2} = 0 \tag{8}$$

where τ_{yield} is the yield stress and $\mu_{Bingham}$ is the viscosity; both of these parameters are calibrated.

In the analysis that follows, the equations are simplified by ignoring centripetal acceleration and entrainment terms and using the frictional rheology to calculate the basal resistance stress. This allows for the derivation of simplified equations that demonstrate the behavior of Dan3D. Only the x-direction equation of motion is considered for this analysis. By making these assumptions, the equation of motion reduces to:

$$\frac{Dv_x}{Dt} = g\sin(\alpha) + gk\frac{\partial h}{\partial x} - g\tan(\varnothing_b)\cos(\alpha) \tag{9}$$

where α is the slope angle.

Through algebraic rearrangement, this equation can be put in the following form:

$$\frac{Dv_x}{Dt} = \frac{g}{\cos(\alpha)}(\tan(\alpha) - \tan(\theta)) + gk\frac{\partial h}{\partial x} \tag{10}$$

The first term on the right hand side captures the gravitational acceleration and basal resistance to movement, similar to a block sliding down an inclined plane. The second term on the right hand side expresses the acceleration due to internal pressure gradients. It is this term that differentiates equivalent fluid models from rigid body models, such as lumped mass models (Heim,

1932). From Eq. 10, it can be seen that Dan3D simulates two mechanisms that drive landslide motion. The mass will accelerate when the slope angle is greater than the friction angle, as in the initial path of many rock avalanches, or when there is a strong enough free-surface gradient ($\frac{\partial h}{\partial x}$ in Eq. 10 and P force on Fig. 3), as in many flowslides. Equation 10 also demonstrates that when a frictional rheology is used and the free surface gradient is small, the mass will only decelerate when the slope angle is less than the friction angle.

Dan3D-Flex

Dan3D and the flexible block model have been coupled in order to simulate extremely rapid, flow-like landslides that have an initially coherent phase of motion (Fig. 2). The coupled model is called Dan3D-Flex, and has been used to simulate a large number of rock avalanche case histories (e.g. Aaron & Hungr 2016b; Castleton et al. 2016; Grämiger et al. 2016; Moore et al. 2017). To couple the two models, the solution algorithm switches from the flexible block model to Dan3D at a user-specified time. As shown in Aaron & Hungr (2016a, b), this parameter can be chosen to correspond with the expected fragmentation mechanism. The geometry and velocity of the flexible block during the final time step are used as the initial conditions for the Dan3D simulation.

Method

Three rock avalanche case histories have been back-analyzed using Dan3D-Flex. These cases were selected to investigate two primary factors that must be considered when analyzing the runout of rock avalanches: (1) disintegration process and (2) the slide path materials. All three cases have similar volumes; however, they differ in initiation mechanism and path materials. Back-analyzing these events provides a way to quantify the effects of these factors.

Two of the three cases were run using both the flexible block model (with Dan3D-Flex) and ignoring the initially coherent portion of motion (with Dan3D). By comparing the results of these cases, the necessity of using the flexible block model in accurately simulating rock avalanche motion can be assessed.

To explore the effects of path materials, the shear strength distribution required to reproduce field observations was assessed for all three cases using the calibration methodology described in Aaron et al. (2016). In this methodology, quantitative fitness metrics are used to assess the quality of a simulation. These metrics can account for a variety of simulation constraints including impact area, velocity and deposit distribution. For each of the case histories, a wide range of parameter combinations were evaluated. This ensured that we explored the entire parameter space and achieved the best possible parameter fitness to all available back-analysis constraints.

We hypothesize the following. If all three cases can be back analyzed using the same rheology and similar back-analyzed strength parameters, then it is possible that a single volume-dependent failure mechanism governs rock avalanche motion, and that mobility can be explained with a general theory that is not site-specific. However, if the rheology and back-analyzed parameters are different for these cases, then it is more likely that different site-specific mobility mechanisms govern the runout of rock avalanches.

Results

The best-fit parameters, defined as the parameters that best reproduce all simulation constraints (e.g. impact area, deposit distribution and velocity), for each of the three case histories are summarized in Table 1. Individual descriptions of the case histories follow in the subsequent sections.

West Salt Creek

The West Salt Creek rock avalanche occurred on May 25th, 2014, and claimed the lives of three people. This landslide released from the northern flank of Grand Mesa, in western Colorado. The event had a complex, two-stage failure mechanism. The first stage included reactivation of an ancient slump block in a unit consisting of shales and marlstones, with an estimated total volume of rock displaced by the slump of 54 Mm^3 (White et al. 2015; Coe et al. 2016). It is thought this reactivation was triggered by a rain-on-snow event (White et al., 2015). The second phase of the failure consisted of rapid evacuation of a rock avalanche from the toe of the displaced slump block (Coe et al. 2016). The rock avalanche had a source volume of approximately 12 Mm^3. The hypothesized initiation mechanism of the rock avalanche, based on Coe et al. (2016), is shown in Fig. 4.

Table 1 Back-analyzed basal resistance parameters for each of the three case histories

Case History	SZ-$\varnothing_b$ (°)	P-$\varnothing_b$ (°)	P-ξ (ms^{-2})	P-τ_{yield} (KPa)	P-$\mu_{Bingham}$ (KPa*s)
West Salt Creek	–	–	–	32	7
Bingham Canyon	10	26	–	–	–
Rautispitz	18	10	300	–	–

The basal rheologies used are summarized in Eqs. 6, 7 and 8. SZ refers to source zone, and P refers to path

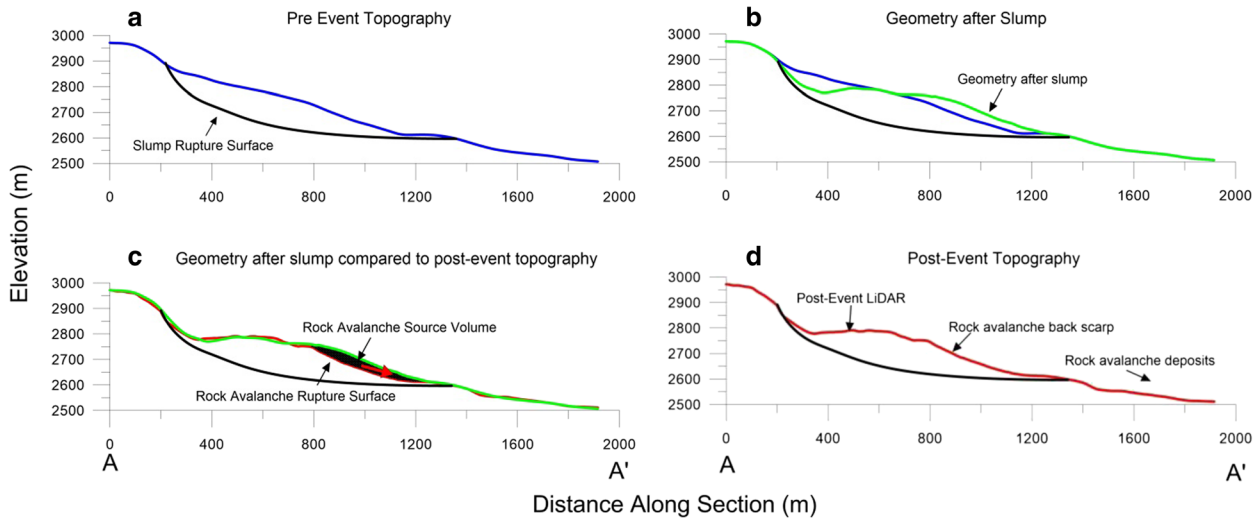

Fig. 4 Failure mechanism for the West Salt Creek Rock Avalanche hypothesized by Coe et al. (2016). Panel **a** shows the topography before failure. The geometry after the slump (*green line* on panel **b** and **c**) was derived from a Dan3D-Flex analysis. Panel **d** shows the topography after the rock avalanche had vacated the source zone. The section line is shown on Fig. 7

White et al. (2015) identified a prehistoric landslide that travelled part of the way down West Salt Creek. White et al. (2015) also noted that the debris of the 2014 event underwent rapid slaking (in the months following the event), which has transformed the shales and marlstones into disaggregated, loose clasts of fine-grained debris. Coe et al. (2016) hypothesized that the surficial sediments present in the West Salt Creek channel likely consisted of a mixture of alluvium and landslide deposits. Based on these observations and hypotheses, it is possible that, after failure, the rock avalanche overran loose fine-grained sediments that had a high degree of saturation from the high precipitation and snowmelt that preceded the rock avalanche.

As can be seen in Fig. 5, the rock avalanche overtopped a 40 m high ridge, and superelevated through three bends along the runout path. Based on these superelevations, White et al. (2015) estimated runout velocities of 37 m/s, 25 m/s and 9 m/s at the three bends (from upstream to downstream, respectively) using the forced vortex equation (e.g. Chow, 1959). Coe et al. (2016) also provided dynamic constraints on the motion of the rock avalanche through interpretation of radiated seismic signals; they estimated that the slide was travelling at an average velocity of 21 m/s.

Lidar data were collected after the event to constrain the post-slide geometry. Pre-event topographic data are available on a 10-m spaced grid. Based on these, the deposit distribution is well-constrained and we derived an accumulation/depletion map (Fig. 7). Immediately down slope of the slump block there is little change in the topography, indicating that either there was no deposition in this zone, or there was erosion of path materials that were later replaced by deposition of rock avalanche debris. Significant deposition begins towards the distal end of the channelized portion of the path. We estimate the volume of material that overtopped the ridge is between 100,000 m^3 and 150,000 m^3 (Fig. 7).

Fig. 5 Overview of the West Salt Creek Rock Avalanche (Photo: J Coe)

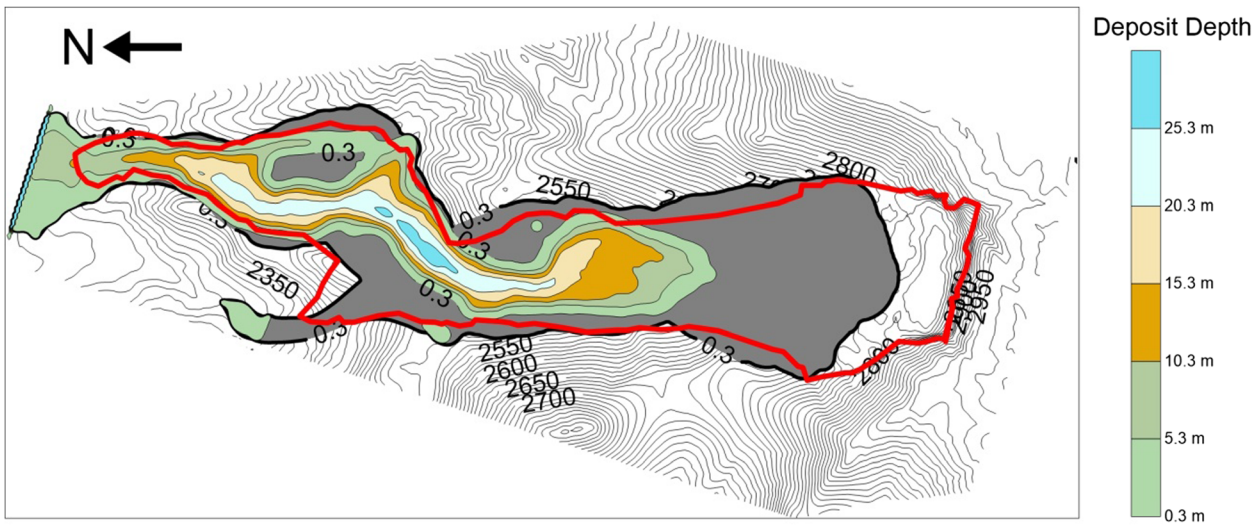

Fig. 6 Final deposit depth and predicted impact area when basal resistance is parameterized with the Voellmy rheology. The red outline shows the observed impact area. A minimum deposit depth value of 0.3 m is necessary due to the solution method used by Dan3D

A back-analysis of the West Salt Creek Rock Avalanche was conducted based on the failure mechanism described by Coe et al. (2016). The 3D rupture surface of the slump block was input into Dan3D-Flex, and a frictional rheology was used to simulate initial rotational failure. We used 7015 columns to represent the failed mass, and the mass was kept rigid throughout the entire simulation. The friction angle was adjusted by trial-and-error until the back-tilted portion at the top of the slope best matched the post-slide LiDAR surface. The results of this back-analysis are shown in Fig. 4. The back scarp of the rock avalanche is visible on the post-slide LiDAR, and this was combined with the final Dan3D-Flex geometry to create a 3D rupture surface for the second phase of motion (i.e. initiation of the rock avalanche). This process is shown schematically in Fig. 4. Our reconstruction resulted in a modelled rock avalanche source volume of 12 Mm^3, very close to that estimated from the accumulation/depletion map.

Initially, we used the Voellmy rheology to parameterize the basal resistance force. The best fit results, obtained by testing 400 different parameter combinations, are shown in Fig. 6. As can be seen in Fig. 7, no combination of friction coefficient and turbulence parameter can simultaneously reproduce the overtopping of the ridge and the distal runout extent. Additionally, when material is predicted to overtop the ridge, it does not deposit in the correct location.

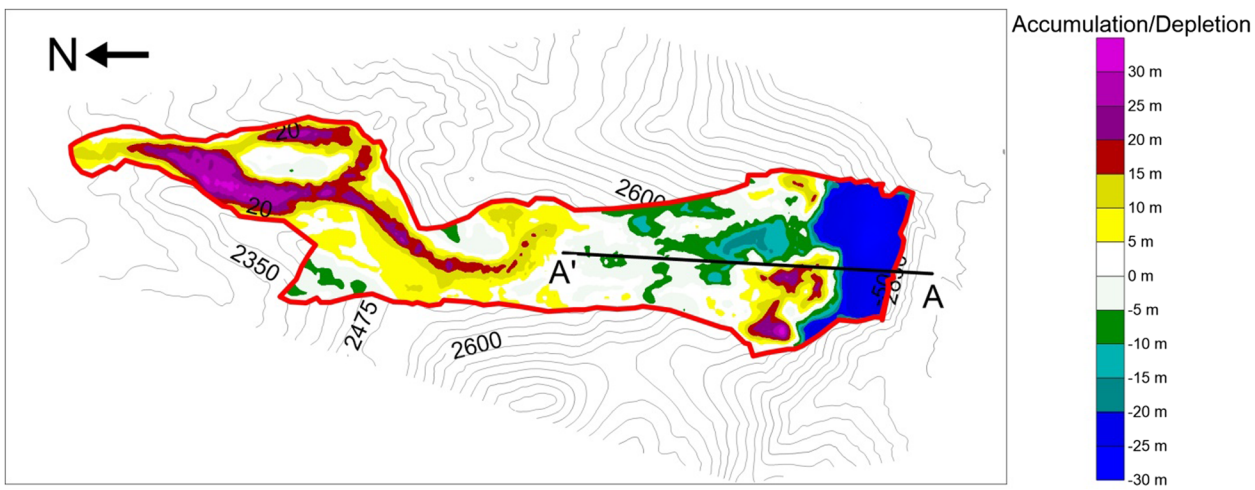

Fig. 7 West Salt Creek Rock Avalanche accumulation and depletion map. Coe et al. (2016) noted that the estimated vertical error of the digital elevation data is ± 4.72 m. The section line refers to Fig. 4

To overcome these shortcomings, we next tested the Bingham rheology. This rheology is appropriate to simulate rapid shearing of fine-grained material, which in the present case represents the saturated, fine-grained material along the valley floor that was overridden by the rock avalanche. The material within the body of the rock avalanche had high frictional strength (Coe et al., 2016). The results of a sensitivity analysis using the Bingham rheology are shown in Fig. 8. As can be seen in Fig. 8, a τ_{yield} =32 KPa and $\mu_{bingham}$ = 7 KPa*s provides the best compromise between simulating both the impact area and deposition on the 40-m high ridge (based on the accumulation depletion map, we expect that the volume deposited on the ridge is between 100,000 m^3 and 150,000 m^3). The simulation results for this best-fit combination are shown in Fig. 9; we obtained good agreement between field observations and model results, both in terms of impact area and deposit thickness distribution. Runout velocities predicted by the model are approximately 30% higher than the maximum velocities estimated by White et al. (2015); however, they broadly agree with the average velocity estimated by Coe et al. (2016).

There are two reasons for the improved results when basal resistance is parameterized with the Bingham rheology. The first is that centripetal accelerations do not increase basal resistance (as in the Voellmy rheology); so the flowing mass expends less momentum overtopping the ridge. The second is that deposition is now controlled by both flow depth and slope angle, as opposed to the frictional and Voellmy rheologies, where deposition is controlled by slope angle alone. This allows the mass to deposit both on the steep overtopped ridge, as well as at the distal toe. These two factors provide strong justification for the use of the Bingham rheology to simulate the West Salt Creek rock avalanche.

Bingham Canyon

The Bingham Canyon rock avalanches were a series of two rock avalanches that occurred on April 10th, 2013, in Utah, USA, at the Bingham Canyon mine (Fig. 10). The mine is one of the largest in the world, and debris from the two landslides filled the pit bottom with waste and destroyed heavy equipment. Most of the data associated with this event is privately owned, and is currently unavailable for researchers. The analysis presented here is based on public data sources and an aerial topographic survey described by Moore et al. (2017).

Both Bingham Canyon rock avalanches initiated along a highly persistent basal fault dipping 21° due west (Fig. 10). This fault extends from the toe of the source area to near the crown. Only a small volume of material was deposited in the source zone, which indicates that the ultimate strength along the basal fault was very low.

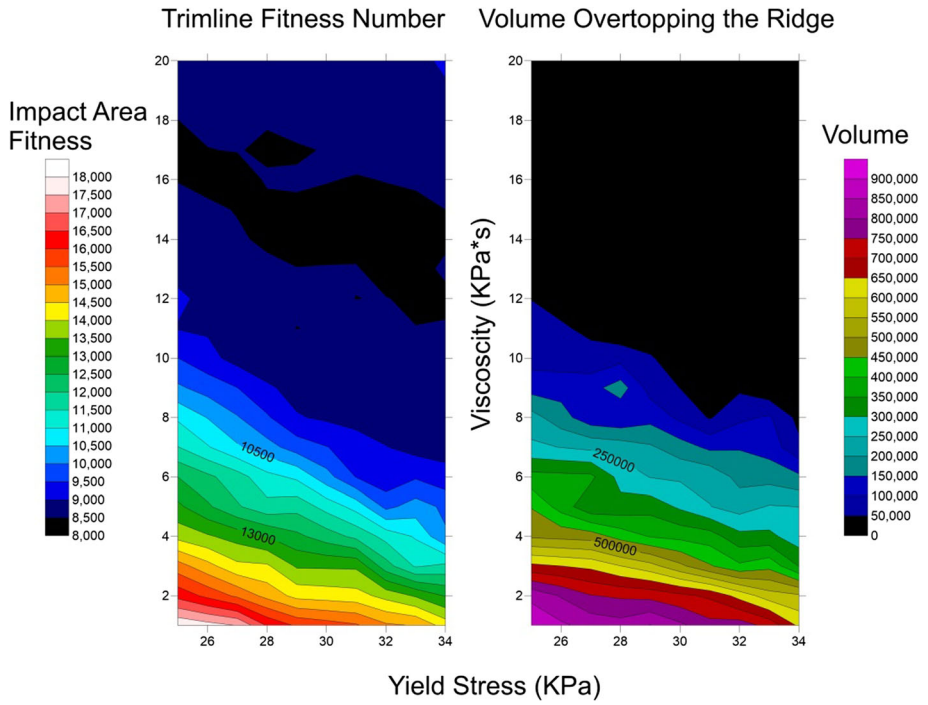

Fig. 8 Results of the sensitivity analysis used to determine the best-fit Bingham parameters for the West Salt Creek rock avalanche. Impact area fitness is calculated using a dimensionless number that measures the misfit between a user specified impact area and the simulated impact area. Lower numbers indicate better fitness (a value of zero indicates perfect agreement between observed and simulated impact area). The best compromise between simulating the observed impact area and deposit distribution is found for τ_{yield} =32 KPa and $\mu_{bingham}$ = 7 KPa*s. Volume is in m^3

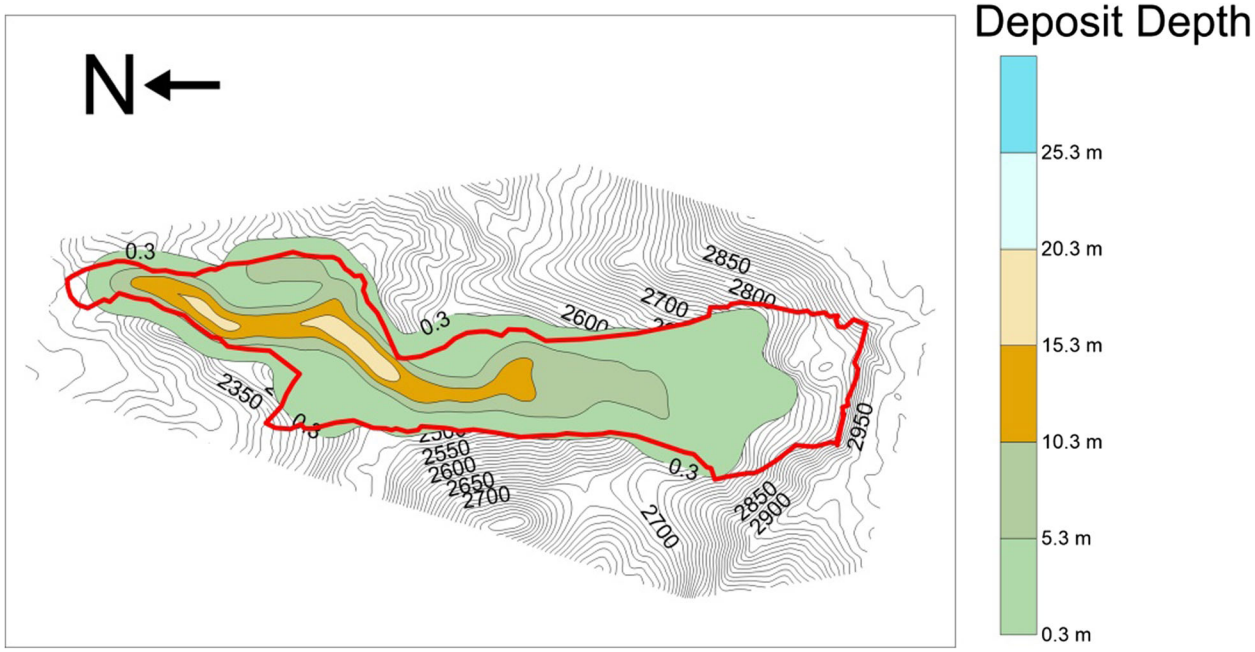

Fig. 9 Predicted impact area and simulated deposit depths when basal resistance is parameterized with the best fit Bingham rheology. The red outline shows the observed impact area. A minimum deposit depth value of 0.3 m is necessary due to the solution method used by Dan3D

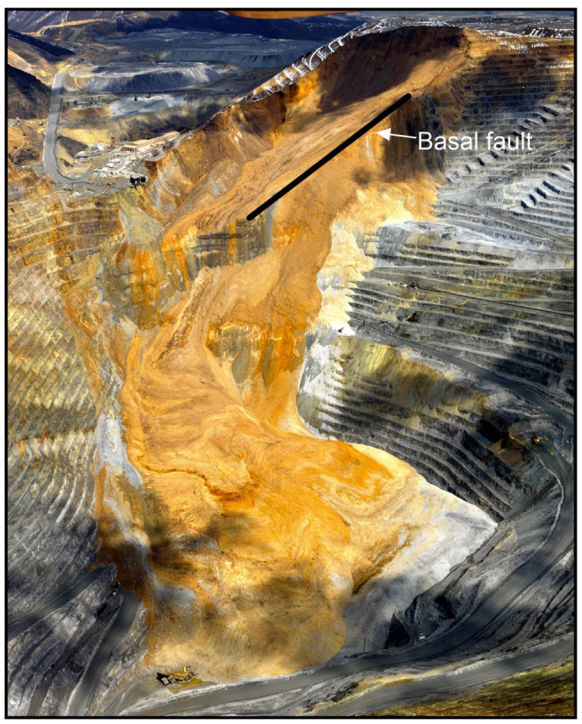

Fig. 10 Overview of the Bingham Canyon rock avalanche. Very little material is left on the rupture surface in the source zone, and there does not appear to be any runup at the distal toe. Modified from Pankow et al. (2014)

In Fig. 10, it can be seen that two different types of debris are visible in the deposit. The grey debris consists of bedrock that failed during the first rock avalanche, while the predominantly orange debris is composed of a higher proportion of waste rock, which failed as the second rock avalanche.

Moore et al. (2017) constructed a post-event digital elevation model (DEM) based on their aerial topographic survey. A pre-event DEM was then derived from the post-event DEM based on a manual reconstruction guided by high-resolution, pre-event aerial photographs. This topographic reconstruction resulted in a total estimated volume of the two rock avalanches of 52 Mm^3. Moore et al. (2017) estimated that 30 Mm^3 failed during the first rock avalanche and 22 Mm^3 failed during the second rock avalanche.

The back-analysis presented here was first summarized by Moore et al. (2017). The present work focuses on the values determined for the back-analyzed parameters in the context of rock avalanche movement mechanisms, as well as highlighting the necessity of simulating initially coherent motion using Dan3D-Flex. We used 3609 columns to represent the phase 1 sliding mass, and 4001 columns to represent the phase 2 sliding mass. For the phase 1 simulations, the rigid motion distance was selected to correspond with fragmentation occurring when the mass vacates the source zone and interacts with the rugged topography on the benches. For the phase 2 simulations, it was selected to correspond with the phase 2 sliding mass impacting the scarp vacated by the phase 1 debris. The basal resistance force was parameterized using two frictional rheologies, one in the source zone and one for the pit walls and floor (Fig. 11). The two friction angles that govern these rheologies were then calibrated. Two field observations proved critical when calibrating these rheologies. Firstly, the strength of the basal fault in the source zone had to be low enough so that all the material vacated the planar rupture surface. Secondly, Fig. 10 shows that there was very little runup on the distal pit wall, indicating that the mass did not energetically runup and fall back into the pit.

The best-fit results using Dan3D-Flex are shown in Fig. 11a. These simulations use a friction angle of 10° in the source zone and 26° along the runout path (Table 1). As noted by Moore et al. (2017), this parameter combination reproduces velocity estimates based on field measurements of superelevation and runup. These simulations reproduce the two key field observations noted above: (1) little volume is simulated to remain on the planar rupture surface, and (2) no runup is simulated at the toe.

The best-fit results of a back analysis for the first rock avalanche not using the flexible block model are shown in Fig. 11b. Excessive spreading around the source zone is predicted by the model, resulting in a poor reproduction of the observed impact area. The runout distance is also underpredicted when the same friction angles are used as in the Dan3D-flex simulations. Selecting a lower friction angle that reproduces the distal runout distance leads to even more excessive lateral spreading.

Rautispitz

The Rautispitz rock avalanche is a prehistoric landslide that occurred in the Glarner Alps of eastern Switzerland. This rock avalanche was recently analyzed by Nagelisen et al. (2015), and cosmogenic nuclide surface exposure dating indicated an age of 12.6 ± 1 ka. The Rautispitz rupture surface is a 33° dip slope. The rock avalanche initiated as a planar sliding failure with volume of approximately 91 Mm^3. After the rock avalanche traversed down the source slope, it ran up the opposing valley wall and spread out over the valley floor (Fig. 12). Landslide deposits dammed the Sulzbach River, creating Lake Obersee and projected a tongue of debris that travelled several kilometers down to the village of Naefels (Fig. 12) (Nagelisen et al., 2015).

A Dan3D back analysis of the Rautispitz rock avalanche was conducted by Nagelisen et al. (2015); however, this analysis was performed before the creation of Dan3D-Flex. Thus, due to the inability of simulating an initially coherent phase of motion, Nagelisen et al. (2015) instead had to use varying internal strength, a topographic wall around the source zone, and high basal resistance outside the observed impact area in order to limit undue lateral spreading.

To overcome these deficiencies, the back analysis was rerun using Dan3D-Flex. The topography files used were those created by Nagelisen et al. (2015), who used a post-event DEM to derive an estimate of the pre-event rupture surface. Two material types were used in the back analysis: (1) the frictional rheology was used in the source zone, and (2) the Voellmy rheology was used for the valley floor. A friction angle of 18° was assigned on the source slope (Table 1), consistent with the mechanism of extreme polishing of a planar feature due to high bed-normal stresses (Cruden & Krahn 1978). The rigid motion distance for Dan3D-Flex was selected to correspond to the location where most of the material had vacated the rupture surface, assuming the likely fragmentation mechanism for this rock avalanche was interaction with rugged topography (De Blasio 2011). We used 11,790 columns to represent the failed mass.

The best-fit results of our new back-analysis are shown in Fig. 13. The results are similar to those obtained by Nagelisen et al. (2015); however, the crucial difference between these and the present results is the model parameterization. It was found necessary to use two different rheologies in order to simultaneously reproduce the proximal and distal deposits (Table 1); however, no

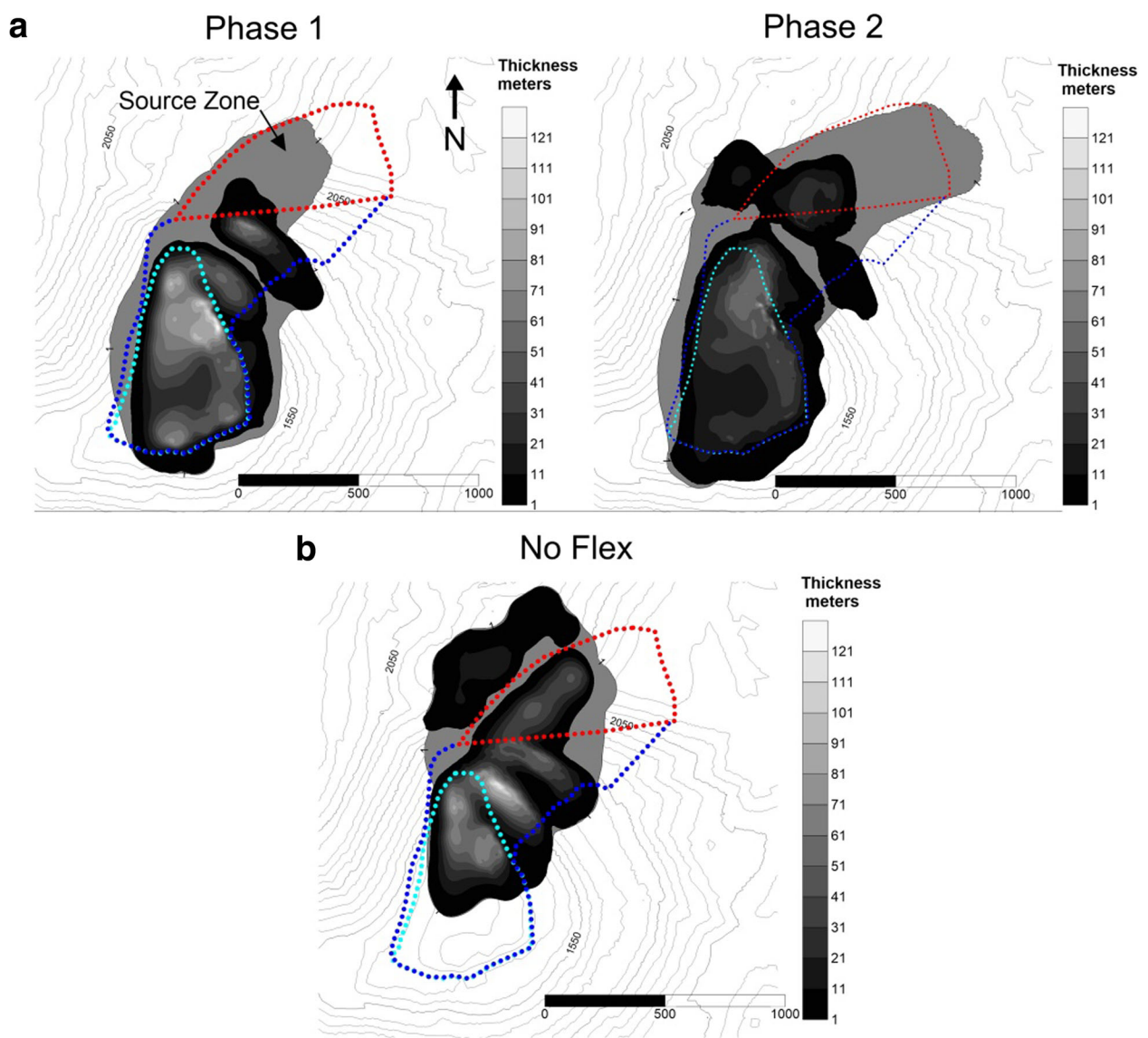

Fig. 11 Simulation results for the two rock avalanche phases of the Bingham Canyon slide (**a**). Simulation results for the first rock avalanche when the flexible block model is not used (**b**); here a large amount of material spills out to the north of the source zone, which is inaccurate. The red outline shows the source zone, the light blue outline shows the final deposit extent and the dark blue line shows the observed impact area. The minimum deposit depth value was specified as 1 m (a minimum deposit depth is necessary due to the solution method used by Dan3D)

extra parameters (or unreal topographic barriers) were needed to limit lateral spreading.

Discussion

The three back analyses demonstrate that the accuracy of rock avalanche runout models can be greatly improved by accounting for the initially rigid phase of motion. These back analyses also show that the basal shear strength and resulting dynamic behavior can be explained by the character of the path materials.

The necessity of accounting for the initial, coherent phase of landslide motion in runout models manifests itself differently in each of our three analyzed case histories. For the Rautispitz rock avalanche, reasonable simulation results could be attained without the flexible block model; however, this required a parameterization that would be difficult to predict *a priori*. As shown by Nagelisen et al. (2015), attaining reasonable results using the unmodified version of Dan3D required assigning a high friction angle outside the observed impact area in order to limit lateral spreading. In effect, the user prescribed the amount of lateral spreading that is allowed, as opposed to letting the numerical model predict this behaviour. This is undesirable because it removes one of the major advantages of simulating landslide motion over three-dimensional terrain. As shown in Fig. 13, Dan3D-Flex enabled a

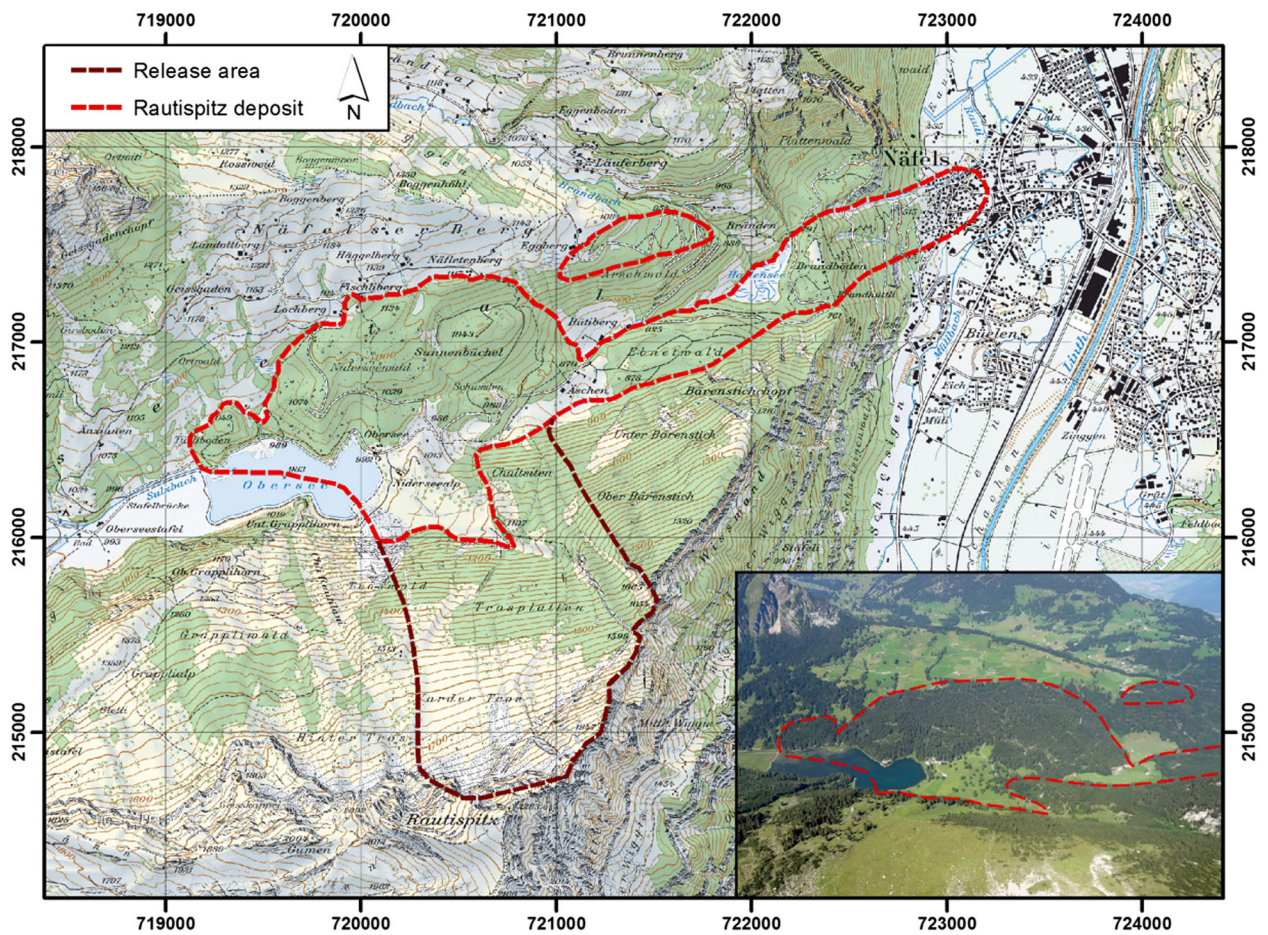

Fig. 12 Mapped release and deposit area extents for the Rautispitz rock avalanche (Nagelisen et al. 2015); inset photo from Rautispitz summit looking north over deposits near Lake Obersee. Coordinates are in meters of the Swiss grid system; map grid interval = 1 km

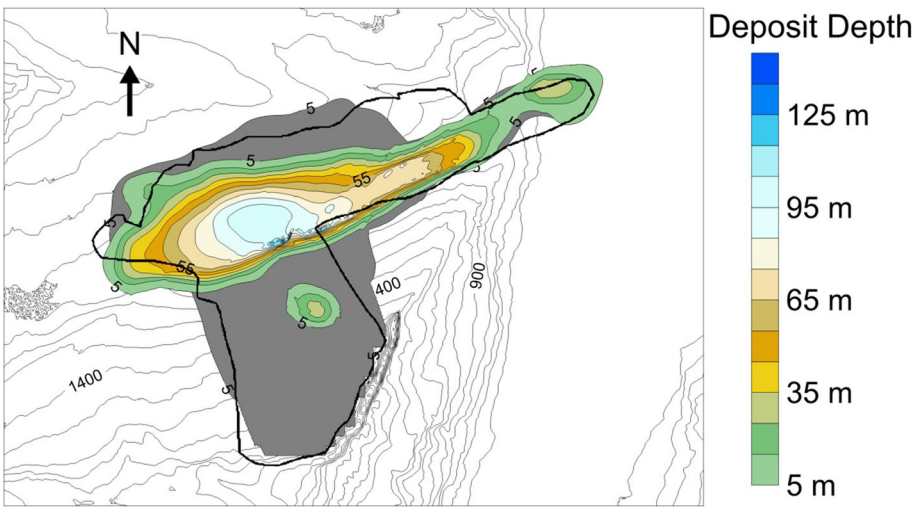

Fig. 13 Rautispitz calibrated results using Dan3D-Flex. The use of Dan3D-Flex enabled a model parameterization that could be anticipated before the event happened. The black outline shows the observed impact area, and a minimum deposit depth of 5 m was used

simple parameterization of basal resistance, comparable to that used for previously successful back analyses of rock avalanches. Therefore, these results can be used to aid forward-analysis. The use of the flexible block model to simulate the initially coherent stage of motion is consistent with the movement mechanism governing this stage of motion, and the one additional parameter (the distance travelled as a coherent block) can be assessed a priori based on pre-failure topography (Aaron and Hungr, 2016b).

As shown in Fig. 11, a reasonable simulation of the Bingham Canyon rock avalanches is impossible without the flexible block model. No parameterization of basal resistance is able to restrict the initial rock avalanche motion to the low-strength basal fault in the source zone. The use of the flexible block model enables more realistic simulation of this event, as the initial failure mechanism is appropriately reproduced. The distance travelled as a flexible block for the first rock avalanche corresponds to the assumption that the failed mass fragmented when it spilled out of the rupture surface and down the steep, benched pit wall. For the second rock avalanche, the flexible block distance corresponds to fragmentation induced by impact with the steep scarp left behind after the first rock failure. Thus, the user specified flexible block distance for this case could be forecast *a priori* to correspond to these mechanisms.

For West Salt Creek, the flexible block model is not necessary once the rock avalanche initiates; however, in order to simulate the complex failure process hypothesized by Coe et al. (2016), Dan3D-Flex is needed to reproduce the initial rotational slump and the initiation of the rock avalanche. Without this capability, it would be difficult to determine the initial geometry of the long runout portion and test the Coe et al. (2016) failure mechanism. If 3-D limit equilibrium analyses were able to determine the failure mechanism of the West Salt Creek landslide, Dan3D-Flex can be used to assess the initial failure volume of the potential rock avalanche. Forecasting such a mechanism a priori, however, remains challenging.

Although similar in volume, the case histories analyzed in this study have vastly different best-fit basal resistance parameters. The Bingham Canyon rock avalanche is best simulated using two frictional rheologies, one in the source zone and one along the path. The best-fit friction angles are 10° and 26°, respectively. The low friction angle in the source zone likely corresponds to extreme polishing of the planar basal rupture surface due to shearing under high normal stress (Cruden & Krahn 1978; Aaron and Hungr, 2016a). The friction angle along the path corresponds closely to that expected for dry fragmented rock (~30°, Hsu (1975)).

The Rautispitz rock avalanche is best simulated using a frictional rheology in the source zone and a Voellmy rheology for the path. Similar to Bingham Canyon, a low back-analysed friction angle was assumed in the source zone, likely corresponding to shearing from peak to ultimate strength. The back-analyzed Voellmy parameters correspond to rapid undrained loading of loose saturated sediments (Hungr and Evans, 2004).

For West Salt Creek, comparing Figs. 6, 7 and 9 demonstrates that the avalanche could not be well simulated using a Voellmy rheology. Simultaneous reproduction of the runout distance and hill overtopping were only obtained by incorporating a basal rheology governed by a constant yield stress and velocity-dependent resistance. This rheology (Bingham) is appropriate for liquefied, fine-grained materials (Jeyapalan, 1981). The reason that this rheology worked well for this case is that the West Salt Creek rock avalanche likely overrode and liquefied the clayey colluvium that mantled the pre-failure path. A similar style of event was documented by Geertsema et al. (2006).

Back-analyzed resistance parameters required to reproduce the observed field characteristics of the three studied case histories are well explained by the path materials, and it is likely that interaction with path materials is the mechanism governing the runout behavior of many rock avalanches. It is unlikely that any single intrinsic mechanism can explain the contrasting basal shear strength of the West Salt Creek rock avalanche and the Bingham Canyon rock avalanches. Any such mechanism should act similarly for both events; however, after vacating the rupture surface, the Bingham Canyon rock avalanches did not exhibit excessive mobility, whereas the West Salt Creek rock avalanche was highly mobile and not governed by frictional mechanics. Comparison of these two cases demonstrates a spectrum of rock avalanche behavior, corresponding to high- and low-strength path materials. The only volume-dependent mechanism needed to explain their behavior is the reduction in friction angle along the basal surface due to shearing under high normal stress. This fact, combined with the interaction with path material, is likely a mechanism that governs the runout behavior of many large-volume rock avalanches.

Conclusion

Through back-analysis of three rock avalanche case histories, we have demonstrated the importance of accounting for the initially coherent phase of motion in dynamic models. We also derived the basal shear resistance along the runout path required to reproduce bulk characteristics of each of the three cases, and used these results to infer mechanisms of rock avalanche mobility. The present work cannot conclusively prove nor disprove any of the rock avalanche mobility theories. It is likely that multiple mechanisms influence rock avalanche motion; however, the present work demonstrates that the path materials can

exert a strong influence on mobility. Our back-analysis results can be used to derive new observations to further test existing mobility theories. Any successful, universal theory of rock avalanche mobility must be able to account for the fact that the Bingham Canyon rock avalanche experienced high frictional resistance along the runout path, the Rautispitz rock avalanche experienced low frictional resistance on the runout path, and that the basal resistance of the highly mobile West Salt Creek rock avalanche cannot be explained by frictional mechanics alone. The authors consider it unlikely that any rock avalanche intrinsic mechanism will be able to explain these three contrasting observations.

Acknowledgements
This work was supported by a graduate scholarship provided by The Natural Sciences and Engineering Research Council of Canada, as well as scholarships provided by the Department of Earth, Ocean and Atmospheric Sciences at The University of British Columbia. We thank Francis Rengers, Rex Baum, Janet Slate and two anonymous reviewers for their constructive comments that improved the manuscript.

Authors' contributions
JA carried out the analysis and drafted the manuscript. SM helped with the numerical modelling and helped draft the manuscript. JM collected data and performed some of the analysis for Bingham Canyon and Rautispitz. JC collected data and provided guidance on the analysis of the West Salt Creek rock avalanche. OH helped draft the manuscript. All authors read and approved the final manuscript.

Competing interests
The authors declare that they have no competing interests.

Author details
[1]Department of Earth, Ocean and Atmospheric Sciences, University of British Columbia, 2020 - 2207 MainMall, Vancouver, British Columbia V6T 1Z4, Canada. [2]Department of Geology and Geophysics, University of Utah, 115 South 1460 East, Salt Lake City, UT 84112, USA. [3]U.S. Geological Survey, Denver Federal Center, MS 966, Denver, Colorado 80225, USA.

Received: 19 October 2016 Accepted: 28 January 2017
Published online: 07 February 2017

References

Aaron, J and Hungr, O. 2016a. Dynamic analysis of an extraordinarily mobile rock avalanche in the Northwest Territories, Canada. *Canadian Geotechnical Journal* 53:899–908.

Aaron, J and Hungr, O. 2016b. Dynamic simulation of the motion of partially-coherent landslides. *Engineering Geology* 205: 1–11.

Aaron J, Hungr, O, & McDougall, S. 2016. Development of a systematic approach to calibrate equivalent fluid runout models. In: Aversa, S, Cascini, L, Picarelli, Scavia, C (eds) Proceedings of the 12th international symposium on landslides, Napoli, Italy, 12-19 June 2016, 285-293.

Bouchut, F, Mangeney-Castelnau, A, Perthame, B and Vilotte, J. 2003. A new model of Saint Venant and Savage–Hutter type for gravity driven shallow water flows. *Comptes Rendus Mathematique* 336(6):531–536.

Bowman, ET, Take, WA, Rait, KL and Hann, C. 2012. Physical models of rock avalanche spreading behaviour with dynamic fragmentation. *Canadian Geotechnical Journal* 49:460–476.

Cascini, L, Cuomo, S, Pastor, M, Sorbino, G and Piciullo, L. 2014. SPH run-out modelling of channelized landslides of the flow type. *Geomorphology* 214:502–513.

Castleton, JJ, Moore, J, Aaron, J, Christl, M, and Ivy-Ochs, S. 2016. Dynamics and legacy of 4.8 ka rock avalanhce that dammed Zion Canyon, Utah, USA. *GSA Today* 26(6):4–9.

Chow, V. 1959. *Open-Channel Hydraulics*. New York: McGraw-Hill Book Co.

Coe, J, Baum, RL, Allstadt, KE, Kochevar, BF, Jr., Schmitt, RG, Morgan, ML, White, JL, Stratton, BT, Hayashi, TA and Kean, JW. 2016. Rock-avalanche dynamics revealed by large-scale field mapping and seismic signals at a highly mobile avalanche in the West Salt Creek valley, western Colorado. *Geosphere* 12(2):607–631.

Corominas, J. 1996. The angle of reach as a mobility index for small and large landslides. *Canadian Geotechnical Journal* 33: 260–271.

Cruden, D, and Krahn, J. 1978. Frank Rockslide, Alberta, Canada. In *Rockslides and Avalanches, Vol 1 Natural Phenomena*, ed. B. Voight, 97–112. Amsterdam: Elsevier Scientific Publishing.

Dai, ZL, Huang, Y, Cheng, HL, and Xu, Q. 2014. 3D numerical modeling using smoothed particle hydrodynamics of flow-like landslide propagation triggered by the 2008 Wenchuan earthquake. *Engineering Geology* 180:21–33.

De Blasio, FV. 2011. Dynamical stress in force chains of granular media traveling on a bumpy terrain and the fragmentation of rock avalanches. *Acta Mechanica* 221(3-4):375–382.

De Blasio, FV, and Crosta, GB. 2015. Fragmentation and boosting of rock falls and rock avalanches. *Geophysical Research Letters* 42:8463–8470.

Geertsema, M, Hungr, O, Schwab, J, and Evans, S. 2006. A large rockslide–debris avalanche in cohesive soil at Pink Mountain, northeastern British Columbia, Canada. *Engineering Geology* 83(1-3):64–75.

Grämiger, LM, Moore, J, Vockenhuber, C, Aaron, J, Hajdas, I, and Ivy-Ochs, S. 2016. Two early Holocene rock avalanches in the Bernese Alps (Rinderhorn, Switzerland). *Geomorphology* 268:207–221.

Heim, A. 1932. *Bergsturz und Menschenleben (Landslides and Human Lives), Translated by N. Smermer*. Vancouver: Bitech Press.

Hsu, KJ. 1975. Catastrophic debris streams (Sturzstroms) generated by rockfalls. *Geological Society of America Bulletin* 86: 129–140.

Huang, Y., W.J. Zhang, Q. Xu, X. Pan, and L. Hao. 2012. Run-out analysis of flow-like landslides triggered by the Ms 8.0 2008 Wenchuan earthquake using smoothed particle hydrodynamics. *Landslides* 9: 275–283.

Hungr, O. 1995. A model for the runout analysis of rapid flow slides, debris flows and avalanches. *Canadian Geotechnical Journal* 32: 610–623.

Hungr, O, and Evans, SG. 2004. Entrainment of debris in rock avalanches: an analysis of a long run-out mechanism. *Geological Society of America Bulletin* 116(9):1240–1252.

Hungr, O, and McDougall, S. 2009. Two numerical models for landslide dynamic analysis. *Computers & Geosciences* 35(5):978–992.

Jeyapalan, K. 1981. *Analysis of flow failures of mine tailings impoundments*. Berkeley: University of California.

Johnson, BC, Campbell, CS, and Melosh, HJ. 2016. The reduction of friction in long runout landslides as an emergent phenomenon. *Journal of Geophysical Research, Earth Surface* 121(5):881–889.

Legros, F. 2002. The mobility of long-runout landslides. Engineering Geology 63 (3-4):301–331.

Legros, F. 2006. Landslide Mobility and the Role of Water. In: Evans SG, Mugnozza GS, Strom A, Hermanns RL. (eds) Landslides from Massive Rock Slope Failure. NATO Science Series, 49:233-242. Springer, Dordrecht.

Li, T. 1983. A mathematical model for predicting the extent of a major rockfall. *Zeitschrift fur Geomorphologie Neue Folge* 27:473–482.

Loew, S, Gschwind, S, Gischig, V, Keller-Singer, A, Valenti, G. 2017. Monitoring and early warning of the 2012 Preonzo catastrophic rockslope failure. *Landslides* 14:141-154.

Lucas, A, Mangeney, A, and Ampuero, JP 2014. Frictional velocity-weakening in landslides on Earth and on other planetary bodies. *Nature Communications* 5: 3417.

Manzanal, DV, Drempetic, B, Haddad, M, Pastor, M, Stickle, M, and Mira, P. 2016. Application of a new rheological model to rock avalanches: An SPH approach. *Rock Mechanics and Rock Engineering* 49(6):2353–2372.

McDougall, S. 2006. A New Continuum Dynamic Model For the Analysis of Extremely Rapid Landslide Motion Across Complex 3D Terrain. PhD Thesis, University of British Columbia, Vancouver, Canada.

McDougall, S, and Hungr, O. 2004. A model for the analysis of rapid landslide motion across three-dimensional terrain. *Canadian Geotechnical Journal* 41: 1084–1097.

McDougall, S, and Hungr, O. 2005. Dynamic modelling of entrainment in rapid landslides. *Canadian Geotechnical Journal* 42:1437–1448.

Melosh, HJ. 1979. Acoustic fluidization: a new geologic process? *Journal of Geophysical Research* 84:7513–7520.

Moore, J, Pankow, K, Ford, S, Koper, K, Hale, M, Aaron, J, Larsen, C. 2017. Dynamics of the Bingham Canyon rock avalanches, Utah, USA. Journal of Geophysical Research: Earth Surface. (in press).

Nagelisen, J, Moore, J, Vockenhuber, C, and Ivy-Ochs, S. 2015. Post-glacial rock avalanches in the Obersee Valley, Glarner Alps, Switzerland. *Geomorphology* 238:94–111.
Nicol, D, Jordan, P, Boyer, D, and Yonin, D. 2013. *Johnsons landing landslide hazard and risk assessment, Regional District of Central Kootenay.*
Pankow, K, Moore, J, Hale, M, Koper, K, Kubacki, T, Whidden, K, and McCarter, M. 2014. Massive landslide at Utah copper mine generates wealth of geophysical data. *GSA Today* 24(1): 4–9.
Pastor, M, Haddad, B, Sorbino, G, Cuomo, S and Drempetic, V. 2009. A depth-integrated, coupled SPH model for flow-like landslides and related phenomena. *International Journal for numerical and analytical methods in Geomechanics* 33: 143–172.
Pirulli, M. (2005) Numerical Modelling of Landslide Runout. PhD thesis, Politecnico Di Torino, Turin, Italy.
Pitman, EB, Nichita, C, Patra, A, Bauer, A, Sheridan, M and Bursik, M. 2003. Computing granular avalanches and landslides. *Physics of Fluids* 15(12):3638.
Savage, S. B. & Hutter, K. 1989. The motion of a finite mass of granular material down a rough incline. Journal of Fluid Mechanics 199: 177–215.
Scheidegger, A. 1973. On the prediction of the reach and velocity of catastrophic landslides. *Rock Mechanics* 5: 231–236.
White, J, Morgan, M & Berry, K. 2015. The West Salt Creek Landslide : A Catastrophic Rockslide and Rock/Debris Avalanche in Mesa County, Colorado, Colorado Geological Survey Bulletin 55, 45 p.
Whittall, JR, Eberhardt, E & McDougall, S. 2016. Runout analysis and mobility observations for large open pit slope failures. Canadian Geotechnical Journal (accepted).